RESEARCH ARTICLE

CrossMark

Green synthesis of gold nanoparticles using *Artemisia dracunculus* extract: control of the shape and size by varying synthesis conditions

Stanisław Wacławek[1] · Zuzanna Gončuková[1] · Kinga Adach[1] · Mateusz Fijałkowski[1] · Miroslav Černík[1]

Abstract

In this study, selective green synthesis of gold nanoparticles (nAu) with the use of Tarragon extract (*Artemisia dracunculus*) was investigated. Characterization of the synthetized nAu was carried out using several techniques including: UV-Vis, SEM, zeta potential analysis, DLS, and ATR-FTIR. Based on measurements of Tarragon extract by HPLC-MS, significant chemical substances participating as reducing and stabilizing agents were identified. FTIR confirmed typical functional groups that could be found in these acids on the nAu surface, such as O-H, C=O and C-O. The effects of various parameters (concentration of Tarragon extract, Au precursor, and initial pH of the synthesis) on the shape and size of the nanoparticles have been investigated. UV-Vis and SEM confirmed the formation of nAu at various concentrations of the extract and Au precursor and showed correlation between the added extract concentration and shift in maximal absorbance towards higher frequencies, indicating the formation of smaller nanoplates. Zeta potential determined at various pH levels revealed that its value decreased with pH, but for all experiments in the pH range of 2.8 to 5.0, the value is below − 30 mV, an absolute value high enough for long-term nAu stability. In order to evaluate nAu catalytic activity, the reduction of 4-nitrophenol to 4-aminophenol by sodium borohydride was used as a model system. The reaction takes place 1.5 times faster on Au-triangles than on Au-spherical NPs.

Keywords Gold nanoparticles · Green synthesis · Selective synthesis · Catalysis · 4-Nitrophenol reduction · Remediation

Introduction

Nanoscale particles (NPs) are omnipresent and can be found in nature as inorganic particles, e.g., dust, aerosols, and clays, or organic particles, e.g., proteins, viruses, organic colloids, and vesicles (Buzea et al. 2007). Nowadays, they can be also acquired synthetically for their subsequent application in various fields, e.g., solar energy conversion (Lenert et al. 2014), remediation (Hrabák et al. 2016; Wacławek et al. 2017), and cancer therapy (Li et al. 2018). The most common characteristics of nanomaterials are their dimensions (the number of external dimensions, which are not confined to the nanoscale range, is generally beneath hundreds of nanometers), size, and shape (Jain 2014).

The main practical applications of nanotechnology can be assorted into the following four groups: (1) nanobiotechnology and nanomedicine, (2) nanomaterials, (3) nanoelectronics, and (4) nanosensors/nanodevices, nanotechnological instrumentation, and nanometrology (Valcárcel Cases and López-Lorente 2014). The last area is associated with analytical science, which has a crucial function in the other three (Valcárcel Cases and López-Lorente 2014). Nanoparticles of Au (nAu) and Ag (nAg) are the most commonly used for biomedical applications and in emerging interdisciplinary areas of nanobiotechnology (Begum et al. 2009).

Nanoparticles have long been acquired both physically and chemically, e.g., by chemical reduction with sodium borohydride, hydrazine hydrate, or ethylene glycol. Application of these chemicals may result in their assimilation on the surface

✉ Stanisław Wacławek
  stanislaw.waclawek@tul.cz

✉ Miroslav Černík
  miroslav.cernik@tul.cz

[1] Centre for Nanomaterials, Advanced Technologies and Innovation, Technical University of Liberec, Studentská 1402/2, 461 17 Liberec 1, Czech Republic

of the NPs, increasing their toxicity (Ha et al. 2010). Recent developments show the decisive character of microorganisms and biological systems (e.g., plant extracts) in the biosynthesis of metallic nanoparticles (Makarov et al. 2014; Kudlek et al. 2017). The bioreduction of metal ions by combining biomolecules found in plant extracts (e.g., vitamins, amino acids, enzymes, polysaccharides, and organic acid salts, such as citrates) is environmentally friendly and does not use harmful and costly chemicals (green chemistry approach) (Nadagouda and Varma 2008). Extracts from plants may act as both reducing and capping agents in the nanoparticle synthesis (Varma 2012; Mohammadinejad et al. 2016; Padil et al. 2016). Current research of the biosynthesis of nanometals using plant extracts has unfolded a fresh era in fast and non-poisonous techniques for the production of nanoparticles; however, the chemical processes are indeed complicated (Shankar et al. 2004; Ankamwar et al. 2005; Wang et al. 2008). For instance, Wang et al. (2008) reported the synthesis of nAu, whereby an electrochemical process applying an amino-terminated ionic liquid was used for ion reduction and nAu stabilization. With this approach, small NPs with an average size of ∼ 2 nm were synthesized.

Sharma et al. (2012) described that tea leaf extract can be used for nAu synthesis and variations in the concentration of the tea leaf extract control the size distribution of the nAu created. Huang et al. (2010) determined that *Bayberry's tannin* extract can be applied at the same time as reducing and protective agents to form nAu with an average size of ∼ 2 nm. Similarly, nAu produced by Suman et al. (2014) and Shankar et al. (2003), with the extract from *Morinda citrifolia* roots and *Pelargonium graveolens* leaves with its endophytic fungus had an average size in the range of 8–17 and 20–40 nm, respectively. Cruz et al. (2010) and Dinakar et al. (2013) synthesized nAg with a size in the range of 15–30 nm from *Lippia citriodora*. Many researchers obtained an anisotropic shape of nAu using plant extracts, e.g., *Camellia sinensis*, *Cucurbita pepo*, *Malva crispa*, *Dioscorea bulbifera*, and fungi extracts, e.g., *Trichoderma viride* and *Neurospora crassa* (Ghosh et al. 2011; Quester et al. 2013; Kalyan Kamal et al. 2014; Chandran et al. 2014; Kumari et al. 2016). Kumari et al. (2016) proved that cell free extract, which is a source of reducing and stabilizing agents, can have an effect on the growth of nAu. Despite a large number of studies involving this green synthesis, there are still many unknown factors, e.g., selection of the proper active substance for reduction and stabilization or for controlling the shape and size of the synthesized NPs.

nAu particles are considered as excellent catalysts (Zhao et al. 2015; Wacławek et al. 2018). One test set-up is the reduction of 4-nitrophenol (4-NP) to 4-aminophenol (4-AP) by sodium borohydride (NaBH$_4$) (Ma et al. 2017), which has been used to study the catalytic activity of metal nanostructures

with different shapes, sizes, and composition. The mechanism of this reduction can be explained by the ability of nAu to transfer the electron from BH$_4^-$ to 4-NP (Zhao et al. 2015; Ma et al. 2017).

In this paper, nAu were prepared by reduction and stabilization with the use of Tarragon extract (*Artemisia dracunculus*). For this, the ideal extraction conditions were examined (influence of the extract and the gold precursor concentration, pH during the synthesis). The resulting extracts were characterized by HPLC/MS/MS analysis, the functional groups for the reduction and stabilization of nAu by ATR-FTIR spectroscopy, and morphology of the synthesized nAu by SEM. Reduction of 4-NP by NaBH$_4$ was used as a model system to evaluate the catalytic activity of different shapes (triangle vs. spherical) and sizes of synthesized nAu.

Materials and methods

Chemicals

Tetrachloroauric(III) acid (99.999%), 4-nitrophenol (99%), and sodium borohydride (99%) all purchased from Sigma-Aldrich; NaOH 0.1 M and sodium hydroxide from LACH-NER, s.r.o., (Czech Republic), and ethanol from VWR BDH Prolabo Chemicals (Belgium) were used in the experiments. MiliQ water (18.2 MΩ cm^{-1}, ELGA, Veolia Water, Marlow, UK) was also used in all of the experiments.

Analytical

UV-Vis spectra of nAu were measured within the wavelength range of 200–1100 nm by an ultraviolet-visible LAMBDA™ 35 UV-Vis spectrophotometer (PerkinElmer, USA) with matched 1-cm quartz cells (cuvettes).

The pH was determined using a pH meter (InLab® Expert Pro-ISM).

The composition of organic compounds contained in the plant extract was measured without separation by FIA-MS in the MRM mode developed on HPLC high-performance liquid chromatography (Dionex UltiMate 3000—Thermo Fisher Scientific).

The composition and morphology of the synthesized nAu were studied using a scanning electron microscope (SEM) with a beam current of between 12 and 40 nA and an acceleration voltage of between 0.02 and 30 kV, with a complete detection system comprising an in-lens energy and angle selective backscatter detector (EsB), a 4-quadrant solid-state backscattered detector (AsB), and a conventional secondary electron detector (Everhardt-Thornley, ZEISS, Ultra/Plus, Germany).

The zeta potential values and dynamic light scattering (DLS) were determined in freshly prepared suspensions by Zetasizer ZS (Malvern Instruments Ltd., UK). Measurements were performed (ten runs each) with autocorrelation functions of 10 s. Each result was the average of triplicate measurements.

Attenuated total reflectance Fourier-transform infrared spectroscopy (ATR-FTIR) spectra were acquired at 4000–700 cm^{-1} (with a resolution of 4 cm^{-1}) using a germanium ATR crystal (NICOLET IZ10, Thermo Scientific, USA) equipped with a single reflection angle 45° horizontal ATR accessory.

Extraction process and experimental design

Tarragon (*A. dracunculus*) extract was prepared from dried herbs (Kawon, Poland) by extraction with ethanol to increase the efficiency of the process (Yee et al. 2015). In short, 0.4 g of Tarragon was extracted in 20 mL of 30 *v*% of ethanol by the microwave digestion system (MAGNUM II, ERTEC, Poland). Based on previous tests, an extraction temperature of 80 °C was chosen as the temperature limit (Fig. S1), which corresponds to a 90 W (30% of the maximum power of the microwave system). After 220 s of heating, the system was cooled down for 400 s. Finally, the extract was filtered with a 0.2-μm pore size filter (nylon Whatman® membrane filters).

Different Tarragon cultivars have already been measured by high-performance liquid chromatography. They can contain flavonoid compounds such as: pentahydroxymethoflavone, estragoniside, glycopyranoside, dihydroxyflavavone, pinocembrin, luteolin, quercetin, rutin, kaempferol, annangenin, dihydroxyflavone, naringenin, trihydroxymethoxyflavanone, trihydroxydimethoxyflavanone, dihydroxymethoxydihydrochalcone, davidigenin, sakuranetin, and phenylpropanoids compounds: chicoric acid, hydroxybenzoic acid, hydroxymethoxycinnamic, chlorogenic acid, caffeic acid, caffeoylquinic acid, and caffeoylquinic acid (Obolskiy et al. 2011). The 12 key biologically active secondary metabolites are coumarins (> 1%), essential oils (0.15–3.1%), and phenolcarbonic and flavonoids acids (Obolskiy et al. 2011). However, this research is mainly focused on the detection of phenolic and flavonoid compounds (Table 1), which are responsible for nanoparticle reduction (Sahu et al. 2016). For instance, in the study by Khezrilu Bandli and Heidari, (2014) seven phenolic compounds were detected in

leaves (gallic acid, p-hydroxy benzoic acid, vanillic acid, p-coumaric acid, syrinjic acid, ferolic acid, sinapic acid).

Synthesis and purification of nAu

Synthesis of nAu was performed in continuously heated and stirred (150 rpm) reactors prepared for this purpose (Fig. S2). Basing on previous work (Das et al. 2011), the process was conducted at a temperature of 80 °C, and if not specified otherwise at a pH of 2.8, HAuCl$_4$ concentration of 0.5 mM, extract concentration of 3% (*v/v*), and reaction time of 15 min. The effects of various extract and precursor (HAuCl$_4$) concentrations, time, and pH were studied. Time varied in the study from 0 to 60 min and extract concentration and precursor concentration from 3 to 5% and 0.05 to 5 mM, respectively. For testing the influence of the pH value from 2.8 to 5, the appropriate amount of 0.1-M NaOH solution was added to the reactor.

Before analysis, nAu were purified by centrifugation at 4600 rpm for 15 min (Hettich Rotanta 460R centrifuge) and washed several times with MilliQ water (Balasubramanian et al. 2010). The effectiveness of the purification was confirmed by UV-Vis analysis (Figs. S3 and S4).

Catalysis studies

The catalytic reduction of 4-NP was conducted in a quartz cuvette (1 mL), wherein 70 μL of 4-NP (1 mM) solution was diluted by 430 μL of milliQ water. The color of the solution changed from colorless to dark yellow after the addition of 340 μL of NaBH$_4$ (63 mM). Immediately after, 160 μL of nAu solution (0.125 mM) was added and the resulting solution was mixed several times by pipetting. The maximum absorbance (at 401 nm) was continuously measured during the experiments and converted to 4-NP concentrations based on the calibration curve. The kinetics of 4-NP reduction were fitted to the pseudo first-order kinetic model:

$$\ln\left(\frac{C}{C_0}\right) = -kt \tag{1}$$

where C and C_0 are the summed 4-NP concentrations at time (t) and $t = 0$, respectively, and k is the pseudo first-order kinetic rate constant.

Table 1 Organic compounds found in *Artemisia dracunculus* extract after microwave digestion

Tannic acid (mg/L)	Ascorbic acid (mg/L)	Salicyic acid (mg/L)	Niacin (mg/L)	Ethyl p-anisate (mg/L)	2–5-DHBA (mg/L)	Caffeic acid (mg/L)	Chlorogenic acid (mg/L)	Rutin (mg/L)
11.65	0.93	1.945	0.226	0.327	0.560	20.95	26.5	17.15

Fig. 1 UV-Vis spectra of nAu determined for different Tarragon extract concentrations (3–5%). The inset shows the change of absorbance intensity on a wavelength with the maximum absorbance at 850 nm (conditions: 0.5-mM HAuCl$_4$; reaction time = 15 min; T = 80 °C)
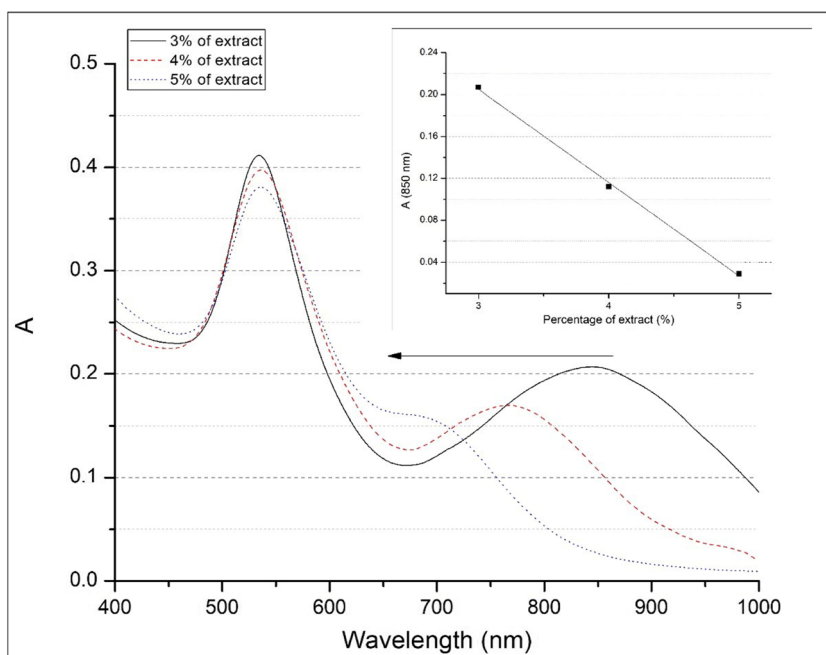
Results and discussion

The effects of various parameters (concentration of Tarragon extract, Au precursor, and initial pH of the synthesis) on the shape and size of the nanoparticles were investigated.

Effect of tarragon dose

The effect of the dose of Tarragon extract (1–5% (*v/v*)) on the size and shape of nAu was evaluated by UV-Vis and SEM analysis and can be observed in Figs. 1 and 2, respectively.

The Tarragon extract concentrations of 1 and 2% were found to be ineffective for the synthesis of nAu (no characteristic peaks were detected in the UV-Vis spectrum), whereas after the addition of 3 to 5%, the color of the samples turned to pinkish violet. In addition to the peak at 530 nm, subsequent peaks at 700 (5% of Tarragon extract), 780 (4% of Tarragon extract), and 850 nm (3% of Tarragon extract) were observed. A correlation was observed between the concentration of the added extract and the shift in the maximum absorbance towards higher frequencies. Indeed, the SEM images confirmed that in the sample with 5% Tarragon extract, the triangle nanoplates were the smallest (with a size of between 35 and 50 nm), compared to 40–75 nm (for 4%) and 80 to 130 nm (for 3%) (see Fig. 2). The shift in the maximum absorbance most likely reflects an increase in nanoprism edge length (Kelly et al. 2003). The band at around 800–920 nm corresponds to a triangular shape with an edge length of less than 100 nm (Fazal et al. 2014). Au nanoplates, with edge lengths of 100–150 nm by seaweed extract synthesized by Liu et al. (2005), have broad SPR bands at 1015 nm. In other literature, the band at 1300 nm correlates to nanoplates with an edge length of 150–200 nm (Millstone et al. 2005). All of the
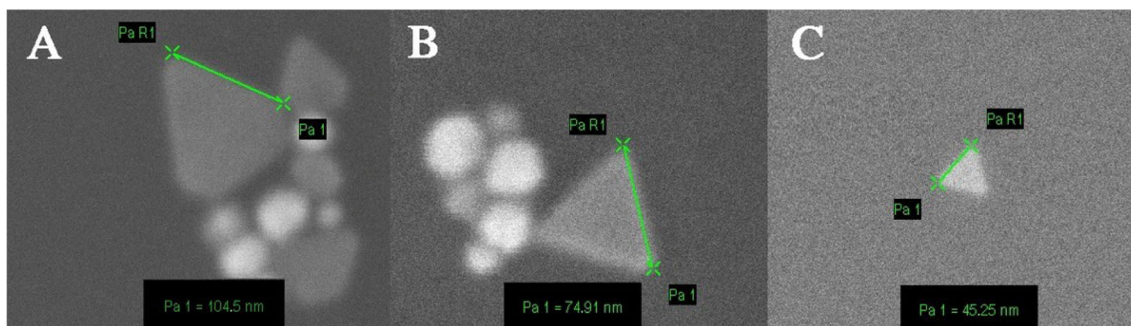

Fig. 2 SEM images of nAu obtained with different Tarragon extract concentrations: **a** 3%, **b** 4%, and **c** 5% (conditions: reaction time = 15 min; 0.5-mM HAuCl$_4$; T = 80 °C)

Fig. 3 UV-Vis spectra of nAu synthesized from different HAuCl$_4$ concentrations. **a** 0.050, **b** 0.275, **c** 0.500, **d** 1.000, **e** 2.750, and **f** 5.000 mM. The inset shows digital images of the synthesized particles as well as the absorbance values at 530 nm (conditions: reaction time = 15 min; 3% Tarragon extract; T = 80 °C)
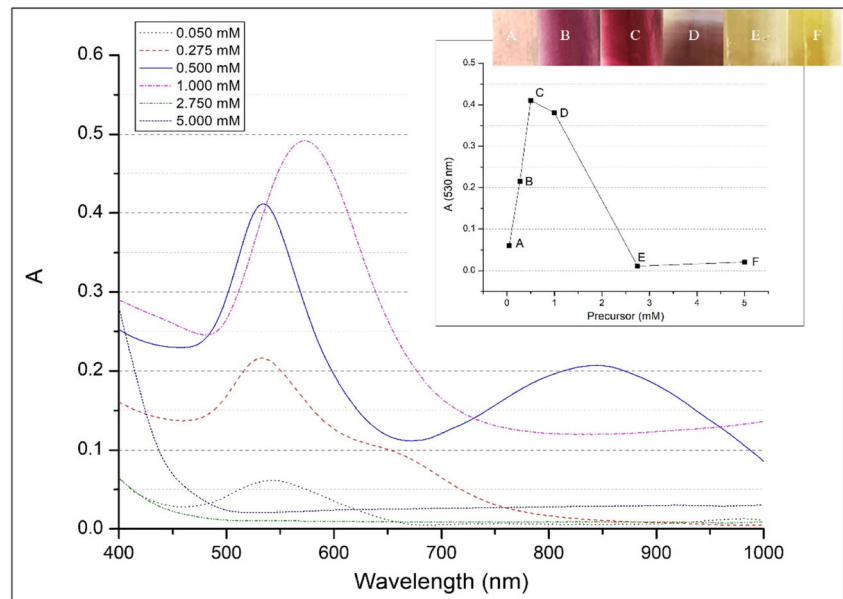
samples also contained spherical nanoparticles with sizes from 30 to 50 nm.

In further experiments (if not specified otherwise), a Tarragon extract dose of 3% was used for the nAu synthesis.

Effect of Au concentration

The influence of different precursor concentrations from 0.05- to 5-mM HAuCl$_4$ on the shape and size of the nanoparticles was investigated. The UV-Vis spectrum (Fig. 3) and SEM images (Fig. 4) show that the precursor concentrations of 0.05 and 0.275 mM were effective in creating spherical nAu. For instance, the sample with 0.05 mM of HAuCl$_4$ possesses a

light pink color (Fig. 3a), and there are no visible triangle nanoplates (Fig. 4a). The nAu synthesized with 0.275 mM of chloroauric acid (Figs. 3b and 4b) possesses a similar shape and size distribution; however, after the addition of a higher precursor dose of 0.5 mM, spherical, hexagonal, and triangular shapes of nAu formed in the reactor. The sample with a dark red color, typical for nAu, was observed for spherical particles with a size of 10 to 50 nm (Fig. 3c). A higher HAuCl$_4$ concentration of 1 mM gave the largest particle size, with spherical (80–100 nm), triangular, and hexagonal (400–550 nm) shapes (Fig. 4d). Due to presence of large nAu, the sample also had dichromatic properties. The second SPR band, which corresponds to the triangle nanoplates, was

Fig. 4 SEM images of nAu synthesized from HAuCl$_4$ concentrations of **a** 0.050, **b** 0.275, **c** 0.500, and **d** 1.000 mM (conditions: reaction time = 15 min; 3% Tarragon extract; T = 80 °C)
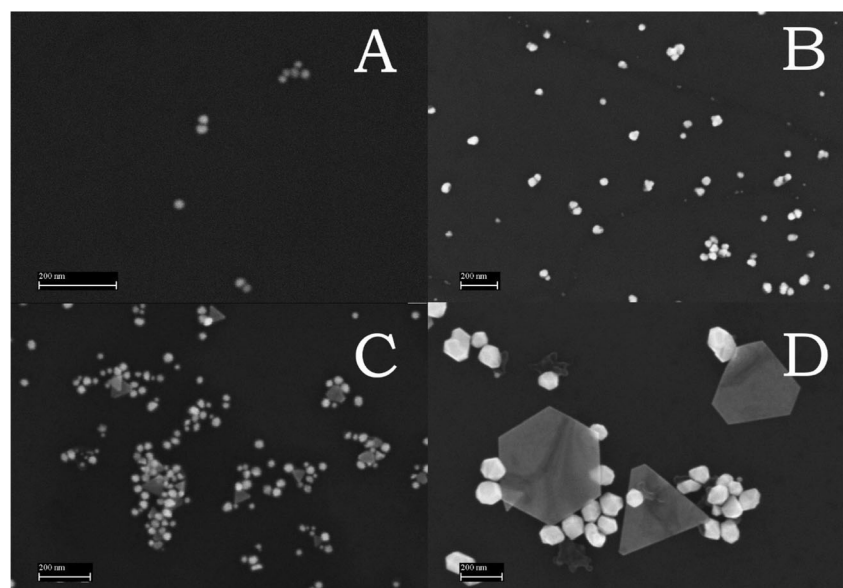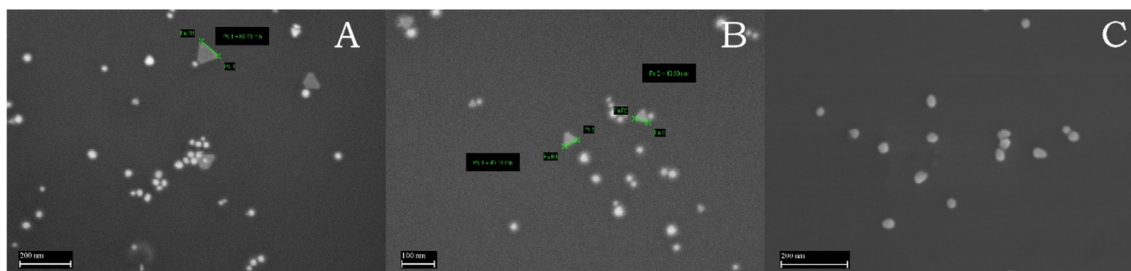
Fig. 5 SEM image of nAu synthesized from 3% of fresh Tarragon extract at pH of 3 (**a**), 4 (**b**), and 5 (**c**)

detected in the NIR region (~ 1412 nm). Furthermore, it is difficult to obtain peaks above a wavelength of 1300 nm due to the truncation of the peaks by the absorbance of water in the IR region (Millstone et al. 2005). In the experiments with even higher precursor concentrations, i.e., 2.75 and 5 mM, the nAu did not form with the given set-up and the color remained yellow without resonance peaks (Fig. 3e, f), indicating that the Au^{3+} ions were not reduced to Au^0.

Effect of pH

According to the literature (Polyakova et al. 2017), the initial pH of $HAuCl_4$ reduction influences the size and shape of the formed nAu. In this study, the pH influence was determined at a $HAuCl_4$ concentration of 0.5 mM and reaction time of 15 min (Fig. S5) at 80 °C. When the initial pH during the synthesis was low (from 2.8 to 4.0), then triangle nanoplates were mainly created. The shape and size of the triangular nanoparticles changed with a subsequent increase in the initial pH value (Fig. 5a–c). The sample with the initial pH value of 2.8 is described above (Figs. 3c and 4c). When the initial pH

value was subsequently increased to a value of 3, 4, and 5, the triangular nAu successively dissipated. Moreover, it was found that when the sample was further alkalinized to a pH of 5, no triangular nanoparticles were formed (Fig. 5c) and the second SPR band disappeared (Fig. 6). Therefore, it can be inferred that the pH value at the beginning of the reaction has a large influence on the shape and size of the synthesized nAu.

Similar experiments were conducted at a $HAuCl_4$ concentration of 1 mM and the same trend was observed (Figs. S6, S7, and S8).

DLS was used to measure the size of the spherical nanoparticles synthesized by the Tarragon extract at a pH of 5. The average nAu measured by DLS was around 42.5 nm (Fig. S9).

Zeta potential

The ζ-potential of nAu reduced by the Tarragon extract slightly decreased with an increase in the initial pH value of the synthesis (Fig. 7). The highest ζ-potential was recorded for the spherical particles synthesized at pH 5.

Fig. 6 UV-Vis spectra of nAu synthesized with different initial pH values (conditions: 0.5 mM $HAuCl_4$; 3% Tarragon extract; 15 min; $T = 80$ °C)
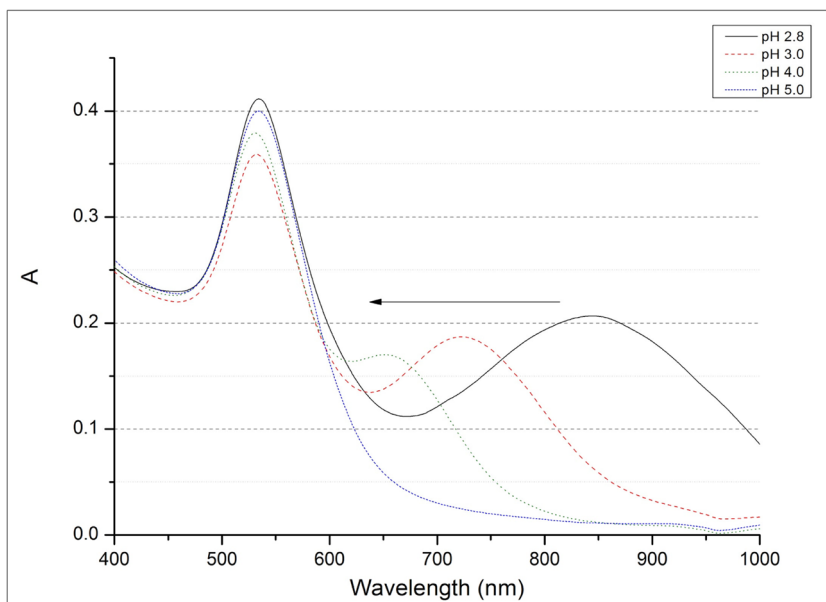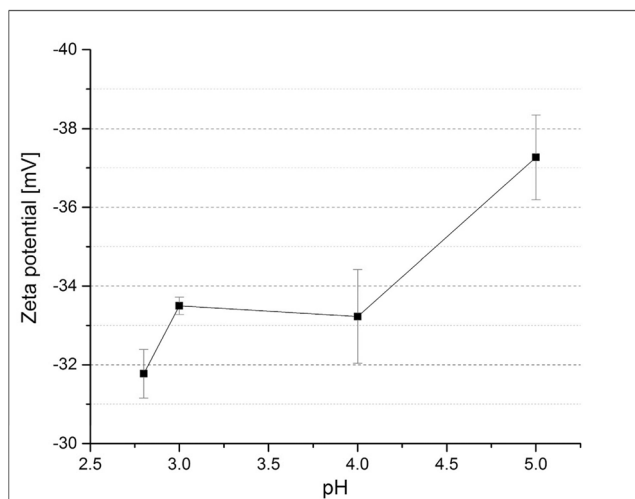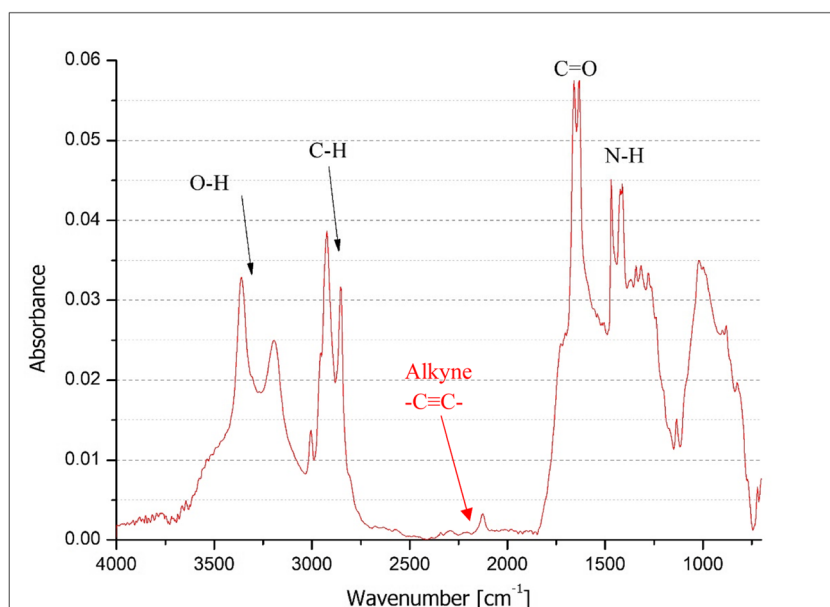
Fig. 7 Values of zeta potential of nAu synthesized from 3% of Tarragon extract and 0.5-mM HAuCl$_4$ at different pH values. The error bars represent standard deviation from three measurements

Spectra of nAu, produced by a reduction of the HAuCl$_4$ precursor (0.5 mM) using 3% of Tarragon extract at a pH of 5.0, clearly showed a large number of peaks in the interval from 3500 to 800 cm^{-1}. The peaks represented typical functional groups O-H, C=O, and C-O at 3400–2400, 1730–1700, and 1320–1210 cm^{-1}, respectively (Singh and Srivastava 2015). These peaks can be found in organic acids, such as ascorbic acid, salicylic acid, caffeic acid, tannic acid, anisate, chlorogenic acid, 2,5-dihydroxybenzoic acid, and also rutin, which were found in this system by HPLC analysis. It can, therefore, be inferred which chemical substances were participating as reducing and stabilizing agents. Moreover, ATR-FTIR analysis showed a broad peak around 1400–1500 cm^{-1}, which attributes to the possible presence of N-H groups.

Catalytic reduction of 4-NP

Au nanoparticles produced at different pH levels had different shapes and sizes. The expected influence of these parameters on catalytic activity was determined by the reduction of 4-nitrophenol (4-NP) to 4-aminophenol (4-AP) using sodium borohydride (NaBH$_4$; Fig. S10 and S11). While without the addition of the nAu catalyst, there was no observed reduction of 4-NP (Fig. S12); after nAu addition, the evolution of a new peak ascribed to 4-AP (at around 310 nm) and a gradual decrease in the absorption peak for 4-NP (at 401 nm) were observed (Fig. S13).

In this work, the reduction of 4-NP to 4-AP could be assumed as a pseudo first-order reaction owing to the presence of NaBH$_4$ in excess (Fig. 9). The pseudo-first-order reaction rate constant for 42.5-nm spherical nAu

The ζ-potential of a colloidal solution can be an indicator of its stability. The greater the absolute value of the ζ-potential, the higher the repulsion between the nanoparticles (Vijayakumar, 2014). A value greater than approximately 30 mV is considered as being high enough for colloidal stability of NPs (Uskoković 2012; Chronopoulou et al. 2016; Padil Vinod et al. 2017).

ATR-FTIR analysis

ATR-FTIR was used to determine the functional groups that take part in the stabilization of nAu (Fig. 8).

Fig. 8 Functional groups of nAu (3% Tarragon extract, 0.5 mM of HAuCl$_4$, and pH 5.0) measured by ATR-FTIR

Fig. 9 The pseudo-first-order re-
action rate constant (k) of 4-NP
reduction over nAu catalysts of
various sizes. The error bars rep-
resent standard deviation from
three measurements. (*spherical
particles synthesized at a pH of 5
with a size of 42.5 nm)
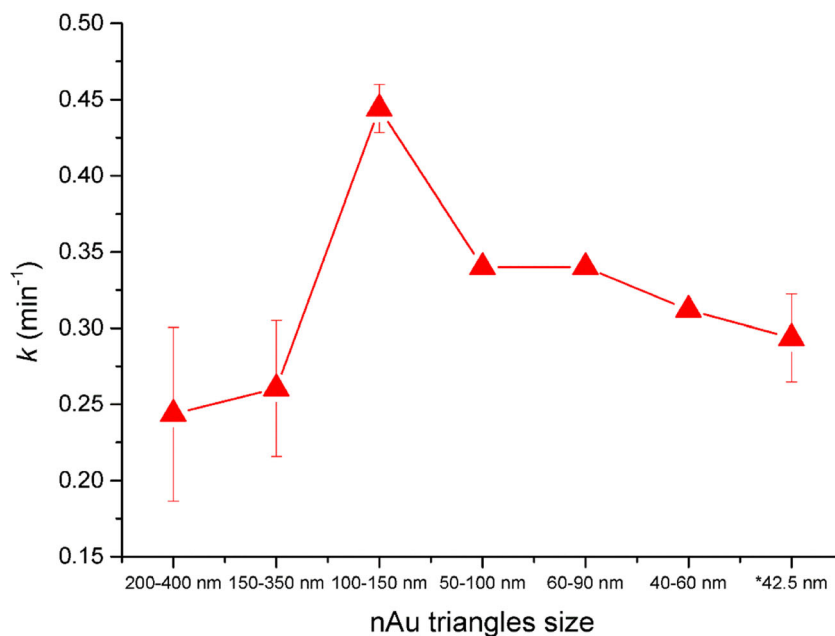
was 0.29 min^{-1}. However, it was observed that with an
increase in the quantity and size of triangle nanoplates,
the k increased until the nAu triangles reached a size of
100–150 nm. Ma et al. (2017) reported that the faster
reduction kinetics on these NPs can be explained by the
different planes that these NPs possess. The catalytic ac-
tivity of metal nanoparticles is strongly dependent on their

size, due to a much greater surface-to-volume ratio (Zeng
et al. 2010). As for larger particles (200–400 nm; 150–
300 nm), the decrease in surface area may cause a de-
crease in the space for the reduction to proceed and there-
fore slower reaction rates. Table 2 shows a comparison of
4-NP reduction with the use of different shapes and sizes
of nAu catalysis.

Table 2 Comparison of 4-NP reduction with addition of various nAu from the literature and this work

Shape of particles	Size of particles (nm)	NaBH$_4$/4-NP/Au (mole ratio)	k (min^{-1})	Ref.
Nanocages	50	1035/3.45/1	2.83	(Zeng et al. 2010)
Nanoboxes	50	1035/3.45/1	1.12	(Zeng et al. 2010)
Spherical	4	516/1.72/1	1.25	(Ma et al. 2017)
Spherical	16	516/1.72/1	0.36	(Ma et al. 2017)
Spherical	40	516/1.72/1	0.23	(Ma et al. 2017)
Stars	40	516/1.72/1	1.78	(Ma et al. 2017)
Stars	117	516/1.72/1	4.36	(Ma et al. 2017)
Templates	80	–	0.0025	(Hajfathalian et al. 2015)
Templates (reduced by a green laser)	100	–	0.04	(Hajfathalian et al. 2015)
Triangles	200–400	504/1.12/1	0.24	[a]
Triangles	150–350	504/1.12/1	0.26	[a]
Triangles	100–150	504/1.12/1	0.44	[a]
Triangles	50–100	504/1.12/1	0.34	[a]
Triangles	60–90	504/1.12/1	0.34	[a]
Triangles	40–60	504/1.12/1	0.31	[a]
Spherical	42.5	504/1.12/1	0.29	[a]

[a] This work

Conclusions

In this study, different conditions for nAu synthesis were applied in order to obtain different sizes and shapes of nAu. It was found that with the decrease of the Tarragon extract concentration from 5 to 3%, the size of triangular nanoparticles increased. The Tarragon extract in the dose of 3% was selected for further experiments with different pH values and different $HAuCl_4$ concentrations. While only spherical nAu were synthesized within a precursor concentration range from 0.05 to 0.275 mM at higher concentrations, spherical, hexagonal, and triangle shapes of NPs were formed. Moreover, the size of the triangle nanoparticles increased. Similarly, while at a low pH (< 4) mainly spherical and triangle shapes of different sizes were create; at a pH of 5 and higher, no triangular NPs were observed.

FTIR analysis revealed the presence of several functional groups on the nAu surface. The FTIR and HPLC-MS analysis confirmed that the reducing and stabilizing properties of Tarragon are due to the presence of hydroxyl, carbonyl, and amino groups originating from its organic acids.

Colloidal suspension of the produced nAu is pretty much stable due to the high absolute value of ζ-potential. The value decreased with increasing pH, but in the pH range of 2.8 to 5.0, the values are below − 30 mV.

A comparison of nAu catalytic activity on the reduction of 4-nitrophenol to 4-aminophenol by sodium borohydride ($NaBH_4$) showed that both triangle and spherical nanoparticles were comparable. The k values indicated that the reaction takes place 1.5 times faster on Au-triangles than on Au-spherical NPs.

References

Ankamwar B, Damle C, Ahmad A, Sastry M (2005) Biosynthesis of gold and silver nanoparticles using *Emblica officinalis* fruit extract, their phase transfer and transmetallation in an organic solution. J Nanosci Nanotechnol 5:1665–1671. https://doi.org/10.1166/jnn.2005.184

Balasubramanian SK, Yang L, Yung L-YL, Ong C-N, Ong W-Y, Yu LE (2010) Characterization, purification, and stability of gold nanoparticles. Biomaterials 31:9023–9030. https://doi.org/10.1016/j.biomaterials.2010.08.012

Begum NA, Mondal S, Basu S, Laskar RA, Mandal D (2009) Biogenic synthesis of Au and Ag nanoparticles using aqueous solutions of Black Tea leaf extracts. Colloids Surf B Biointerfaces 71:113–118. https://doi.org/10.1016/j.colsurfb.2009.01.012

Buzea C, Pacheco II, Robbie K (2007) Nanomaterials and nanoparticles: sources and toxicity. Biointerphases 2:17–71. https://doi.org/10.1116/1.2815690

Chandran K, Song S, Il YS (2014) Effect of size and shape controlled biogenic synthesis of gold nanoparticles and their mode of interactions against food borne bacterial pathogens. Arab J Chem. https://doi.org/10.1016/j.arabjc.2014.11.041

Chronopoulou L, Palocci C, Valentino F, Pettiti I, Wacławek S, Černík M, Petrangeli Papini M (2016) Stabilization of iron (micro)particles with polyhydroxybutyrate for in situ remediation applications. Appl Sci 6:417. https://doi.org/10.3390/app6120417

Cruz D, Falé PL, Mourato A, Vaz PD, Luisa Serralheiro M, Lino ARL (2010) Preparation and physicochemical characterization of Ag nanoparticles biosynthesized by *Lippia citriodora* (Lemon Verbena). Colloids Surf B Biointerfaces 81:67–73. https://doi.org/10.1016/j.colsurfb.2010.06.025

Das RK, Gogoi N, Bora U (2011) Green synthesis of gold nanoparticles using *Nyctanthes arbortristis* flower extract. Bioprocess Biosyst Eng 34:615–619. https://doi.org/10.1007/s00449-010-0510-y

Dinakar S, Isacc Fenn Fenn R, Sobczak-Kupiec A, Basavegowda N (2013) Bioreduction of chloroaurate ions using fruit extract *Punica granatum* (Pomegranate) for synthesis of highly stable gold nanoparticles and assessment of its antibacterial activity. Micro Nano Lett 8:400–404. https://doi.org/10.1049/mnl.2013.0137

Fazal S, Jayasree A, Sasidharan S, Koyakutty M, Nair SV, Menon D (2014) Green synthesis of anisotropic gold nanoparticles for photothermal therapy of cancer. ACS Appl Mater Interfaces 6:8080–8089. https://doi.org/10.1021/am500302t

Ghosh S, Patil S, Ahire M, Kitture R, Jabgunde A, Kale S, Pardesi K, Bellare J, Dhavale DD, Chopade BA (2011) Synthesis of gold nanoanisotrops using *Dioscorea bulbifera* tuber extract. J Nanomater 2011:354793. https://doi.org/10.1155/2011/354793

Ha TH, Kim YJ, Park SH, Buckland BC, Lee AL, Lu Z, Yin Y (2010) Complete separation of triangular gold nanoplates through selective precipitation under CTAB micelles in aqueous solution. Chem Commun 46:3164–3166. https://doi.org/10.1039/c001574a

Hajfathalian M, Gilroy KD, Yaghoubzade A, Sundar A, Tan T, Hughes RA, Neretina S (2015) Photocatalytic enhancements to the reduction of 4-nitrophenol by resonantly excited triangular gold–copper nanostructures. J Phys Chem C 119:17308–17315. https://doi.org/10.1021/acs.jpcc.5b04618

Hrabák P, Homolková M, Wacławek S, Černík M (2016) Chemical degradation of PCDD/F in contaminated sediment. Ecol Chem Eng S 23:473–482. https://doi.org/10.1515/eces-2016-0034

Huang X, Wu H, Liao X, Shi B (2010) One-step, size-controlled synthesis of gold nanoparticles at room temperature using plant tannin. Green Chem 12:395–399. https://doi.org/10.1039/B918176H

Jain PK (2014) Gold nanoparticles for physics, chemistry, and biology. Edited by Catherine Louis and Olivier Pluchery. Angew Chemie Int Ed 53:1197–1197. https://doi.org/10.1002/anie.201309807

Kalyan Kamal SS, Vimala J, Sahoo PK, Ghosal P, Ram S, Durai L (2014) A green chemical approach for synthesis of shape anisotropic gold nanoparticles. Int Nano Lett 4:109. https://doi.org/10.1007/s40089-014-0109-4

Kelly KL, Coronado E, Zhao LL, Schatz GC (2003) The optical properties of metal nanoparticles: the influence of size, shape, and dielectric environment. J Phys Chem B 107:668–677. https://doi.org/10.1021/jp026731y

Khezrilu Bandli J, Heidari R (2014) The evaluation of antioxidant activities and phenolic compounds in leaves and inflorescence of *Artemisia dracunculus* L. by HPLC. J Med Plants 13:41–50

Kudlek E, Silvestri D, Wacławek S, Padil VVT, Stuchlík M, Voleský L, Kejzlar P, Černík M (2017) TiO₂ immobilised on biopolymer nanofibers for the removal of bisphenol A and diclofenac from water. Ecol Chem Eng S 24:417–429. https://doi.org/10.1515/eces-2017-0028

Kumari M, Mishra A, Pandey S, Singh SP, Chaudhry V, Mudiam MKR, Shukla S, Kakkar P, Nautiyal CS (2016) Physico-chemical condition optimization during biosynthesis lead to development of improved

and catalytically efficient gold Nano particles. Sci Rep 6:27575. https://doi.org/10.1038/srep27575

Lenert A, Bierman DM, Nam Y, Chan WR, Celanović I, Soljačić M, Wang EN (2014) A nanophotonic solar thermophotovoltaic device. Nat Nanotechnol 9:126–130. https://doi.org/10.1038/nnano.2013.286

Li S, Jiang Q, Liu S, Zhang Y, Tian Y, Song C, Wang J, Zou Y, Anderson GJ, Han JY, Chang Y, Liu Y, Zhang C, Chen L, Zhou G, Nie G, Yan H, Ding B, Zhao Y (2018) A DNA nanorobot functions as a cancer therapeutic in response to a molecular trigger in vivo. Nat Biotechnol 36:258–264. https://doi.org/10.1038/nbt.4071

Liu B, Xie J, Lee JY, Ting YP, Chen JP (2005) Optimization of high-yield biological synthesis of single-crystalline gold nanoplates. J Phys Chem B 109:15256–15263. https://doi.org/10.1021/jp051449n

Ma T, Yang W, Liu S, Zhang H, Liang F (2017) A comparison reduction of 4-nitrophenol by gold nanospheres and gold nanostars. Catalysts 7:38. https://doi.org/10.3390/catal7020038

Makarov VV, Love AJ, Sinitsyna OV, Makarova SS, Yaminsky IV, Taliansky ME, Kalinina NO (2014) Green' nanotechnologies: synthesis of metal nanoparticles using plants. Acta Nat 6:35–44. https://doi.org/10.1039/c1gc15386b

Millstone JE, Park S, Shuford KL, Qin L, Schatz GC, Mirkin CA (2005) Observation of a quadrupole plasmon mode for a colloidal solution of gold nanoprisms. J Am Chem Soc 127:5312–5313. https://doi.org/10.1021/ja043245a

Mohammadinejad R, Karimi S, Iravani S, Varma RS (2016) Plant-derived nanostructures: types and applications. Green Chem 18:20–52. https://doi.org/10.1039/C5GC01403D

Nadagouda MN, Varma RS (2008) Green synthesis of silver and palladium nanoparticles at room temperature using coffee and tea extract. Green Chem 10:859–862. https://doi.org/10.1039/b804703k

Obolskiy D, Pischel I, Feistel B, Glotov N, Heinrich M (2011) Artemisia dracunculus L. (Tarragon): a critical review of its traditional. J Agric Food Chem 59:11367–11384. https://doi.org/10.1021/jf202277w

Padil VVT, Wacławek S, Senan C, Kupčík J, Pešková K, Černík M, Somashekarappa HM (2017) Gum karaya (Sterculia urens) stabilized zero-valent iron nanoparticles: characterization and applications for the removal of chromium and volatile organic pollutants from water. RSC Adv 7:13997–14009. https://doi.org/10.1039/C7RA00464H

Padil VVT, Wacławek S, Černík M (2016) Green synthesis: nanoparticles and nanofibres based on tree gums for environmental applications. Ecol Chem Eng S 23:533–557. https://doi.org/10.1515/eces-2016-0038

Polyakova NY, Polyakov AY, Sukhorukova IV, Shtansky DV, Grigorieva AV (2017) The defining role of pH in the green synthesis of plasmonic gold nanoparticles using Citrus limon extract. Gold Bull 50:131–136. https://doi.org/10.1007/s13404-017-0203-2

Quester K, Avalos-Borja M, Vilchis-Nestor AR, Camacho-López MA, Castro-Longoria E (2013) SERS properties of different sized and shaped gold nanoparticles biosynthesized under different environmental conditions by Neurospora crassa extract. PLoS One 8:e77486. https://doi.org/10.1371/journal.pone.0077486

Sahu N, Soni D, Chandrashekhar B, Satpute DB, Saravanadevi S, Sarangi BK, Pandey RA (2016) Synthesis of silver nanoparticles using

flavonoids: hesperidin, naringin and diosmin, and their antibacterial effects and cytotoxicity. Int Nano Lett 6:173–181. https://doi.org/10.1007/s40089-016-0184-9

Shankar SS, Ahmad A, Pasricha R, Sastry M (2003) Bioreduction of chloroaurate ions by geranium leaves and its endophytic fungus yields gold nanoparticles of different shapes. J Mater Chem 13:1822–1826. https://doi.org/10.1039/b303808b

Shankar SS, Rai A, Ankamwar B, Singh A, Ahmad A, Sastry M (2004) Biological synthesis of triangular gold nanoprisms. Nat Mater 3:482–488. https://doi.org/10.1038/nmat1152

Sharma RK, Gulati S, Mehta S (2012) Preparation of gold nanoparticles using tea: a green chemistry experiment. J Chem Educ 89:1316–1318. https://doi.org/10.1021/ed2002175

Singh AK, Srivastava ON (2015) One-step green synthesis of gold nanoparticles using black cardamom and effect of pH on its synthesis. Nanoscale Res Lett 10:353. https://doi.org/10.1186/s11671-015-1055-4

Suman TY, Radhika Rajasree SR, Ramkumar R, Rajthilak C, Perumal P (2014) The green synthesis of gold nanoparticles using an aqueous root extract of Morinda citrifolia L. Spectrochim Acta A Mol Biomol Spectrosc 118:11–16. https://doi.org/10.1016/j.saa.2013.08.066

Uskoković V (2012) Dynamic light scattering based microelectrophoresis: main prospects and limitations. J Dispers Sci Technol 33:1762–1786. https://doi.org/10.1080/01932691.2011.625523

Valcárcel Cases M, López-Lorente AI (2014) Gold nanoparticles in analytical chemistry. Elsevier, Amsterdam

Varma RS (2012) Greener approach to nanomaterials and their sustainable applications. Curr Opin Chem Eng 1:123–128. https://doi.org/10.1016/j.coche.2011.12.002

Vijayakumar S (2014) In vitro stability studies on gold nanoparticles with different stabilizing agents. Int J Curr Sci 11:84–93

Wacławek S, Lutze HV, Grübel K, Padil VVT, Černík M, Dionysiou DD (2017) Chemistry of persulfates in water and wastewater treatment: a review. Chem Eng J 330:44–62. https://doi.org/10.1016/j.cej.2017.07.132

Wacławek S, Padil VVT, Černík M (2018) Major advances and challenges in heterogeneous catalysis for environmental applications: a review. Ecol Chem Eng S 25:9–34. https://doi.org/10.1515/ECES-2018-0001

Wang Z, Zhang Q, Kuehner D, Ivaska A, Niu L (2008) Green synthesis of 1–2 nm gold nanoparticles stabilized by amine-terminated ionic liquid and their electrocatalytic activity in oxygen reduction. Green Chem 10:907. https://doi.org/10.1039/b806453a

Yee FY, Periasamy V, Malek SNA (2015) Green synthesis of gold nanoparticles using aqueous ethanol extract of Curcuma mangga rhizomes as reducing agent. In: AIP conference proceedings

Zeng J, Zhang Q, Chen J, Xia Y (2010) A comparison study of the catalytic properties of Au-based nanocages, nanoboxes, and nanoparticles. Nano Lett 10:30–35. https://doi.org/10.1021/nl903062e

Zhao P, Feng X, Huang D, Yang G, Astruc D (2015) Basic concepts and recent advances in nitrophenol reduction by gold- and other transition metal nanoparticles. Coord Chem Rev 287:114–136. https://doi.org/10.1016/j.ccr.2015.01.002